Mini review

Overview on the design and application of magnetically-assisted electrochemiluminescence biosensors

Dandan Liu*, Yanbiao Zhou, Shuman Gao, Ziwen Tang and Ming La*

College of Chemistry and Environmental Engineering, Pingdingshan University, Pingdingshan, Henan 467000, People's Republic of China
*E-mail: liudd0811@126.com (D.L.); mingla2011@163.com (M.L.)

Most of electrochemiluminescence (ECL) biosensors usually require the immobilization of biological recognition elements on the electrode surface by physical adsorption, embedding, self-assembly or covalent bonding. However, such ECL biosensors are limited in practical applications because the modified electrode can only be used once. Magnetically-assisted ECL biosensors have significant advantages in preconcentration and separation of targets in complex samples. More importantly, magnetic sensing systems show high-throughput since magnetic beads or nanoparticles can be produced and preserved in a large-scale dose. In this work, we review the progress in the design and application of magnetically-assisted ECL biosensors based on the difference in the roles of magnetic materials within the sensing system.

1. INTRODUCTION

Electrochemiluminescence (ECL) is a kind of luminescence phenomenon occurring on/near the electrode surface, which is combined with electrochemical reaction and chemiluminescence (CL) reaction [1-3]. ECL biosensors can convert biochemical reactions into ECL signals based on the biomolecular recognition between bioactive molecular recognition substance and ECL signal substance, thus achieving the quantitative detection of target. This method has many advantages, such as strong controllability, high sensitivity, simple instrument and equipment, wide linear range, fast analysis speed, and easy automation. In order to develop efficient methods for the detection of disease-related biomarkers, one of the most critical issues is to design a high-throughput sensing system suitable for large-scale production [4, 5]. Traditional ECL biosensors require the immobilization of probe on the electrode surface by physical adsorption, embedding, self-assembly or covalent bonding, but the pretreatment and reuse of the electrode in this way are cumbersome and time-consuming. Moreover, it

is difficult to achieve high-throughput detection due to the limitation of electrode.

In recent years, capture probes such as antibodies, nucleic acids and polypeptides have been immobilized on the surface of magnetic beads (MBs) as support materials and separation tools through the specific molecular recognition, so as to build biosensors on the solid matrix of MBs [6-8]. This strategy has significant advantages in preconcentration and separation of targets in complex samples under an external magnetic field, thus decreasing the background interferences and showing high sensitivity and selectivity for target detection [9]. Moreover, MBs can be used as the signal labels to increase the detection sensitivity. In this review, we summarized the progress in the design and application of magnetically-assisted ECL biosensors based on the different roles of MBs in the sensing system.

2. MAGNETICALLY-ASSISTED ECL BIOSENSORS

2.1 Electrode substrates

Because of their large surface area and low mass transfer resistance, MBs can be used as the electrode substrates to immobilize organic molecules such as Ruthenium (II) tris(bipyridine) $(Ru(bpy)_3^{2+})$ and biomolecules (e.g. haemoglobin and cytochrome *C*) [10, 11]. Moreover, different MBs-based nanocomposites have been prepared to improve the performances of ECL biosensors (Table 1). For example, Fe_3O_4 NPs were capped into reduced graphene oxide (rGO) to obtain macroporous Fe_3O_4/rGO. The MBs-based core-shell nanostructures have been prepared to facilitate the conjugation of biomolecules. Xu et al. reported an ECL immunosensor for the detection of carbohydrate antigen 125 (CA125) by using MBs as the electrode matrixes and glucose oxidase (GOD) as the enzyme label to produce H_2O_2 [12]. Besides, molecular imprinted polymers (MIPs) can be prepared on the surface of MBs to construct molecularly imprinted ECL (MIP-ECL) assays for various targets, such as bisphenol A, cinchonine and diethylstilbestrol [13, 14]. Moreover, Zhou et al. reported an ECL immunosensor for the detection of HIV-1 antibody with MIPs as the capture probes and HRP as the signal label to increase the ECL signal [15].

In traditional ELISA, few reporters are labeled on the detection antibody, resulting in a low sensitivity. Thus, different materials and nanomaterials have been employed as nanocarriers to immobilize ECL reporters. For example, Li et al. employed poly(diethylenetriaminepentaacetic acid-ethylene glycol) ester dendrimer as the carrier to load the signal labels of luminol molecules [16]. Shao et al. synthesized a ruthenium complex-based metal organic framework (MOF) for the detection of miRNA-141 [17]. Jiang et al. developed a sandwich ECL immunosensor for 5-hydroxymethylcytosine (5hmC) detection with magnetic $Fe_3O_4@SiO_2$ as the matrix for the immobilization of 5hmC antibody [18]. In this work, polyamidoamine (PAMAM) conjugated with avidin and $Ru(bpy)_3^{2+}$ (Ru-PAMAM-adivin) was used as the signal unit. Wang et al. reported an ECL strategy for Vibrio parahaemolyticus (VP) detection by collecting the bacteria with magnetic glassy carbon electrode [19]. In this work, the composite of Ru-AgNPs@GO was used as Faraday cage-type label. The captured VP was recognized by the antibody-labeled Ru-AgNPs@GO that could produce strong ECL and electrochemical signals. Besides, a long-nicked dsDNA polymer from different DNA assembly techniques in-situ generated on

the electrode surface was used as the template for the insertion of ECL luminophores (e.g. perylene derivative and Ru(bpy)$_3^{2+}$) [20, 21].

Table 1. Detection performances of different ECL biosensors by using MBs as the electrode substrates.

Signal label	Target	Linear range	LOD	Ref.
GOD-labeled antibody	CA125	0 ~ 10 mU/mL	10 μU/mL	[12]
Luminol-labeled dendrimer	CA125	0.2 ~ 100 μU/mL	0.032 μU/mL	[16]
Ru-MOFs	miRNA-141	1 fM ~ 10 pM	0.3 fM	[17]
Ru-PAMAM	5hmC	0.1 ~ 30 nM	0.047 nM	[18]
Ru-AgNPs@GO	VP	$10^2 ~ 10^7$ CFU/mL	33 CFU/mL	[19]
AuNPs/DNA	BT63 DNA	0.1 fM ~ 10 nM	0.036 fM	[21]
CeO$_2$@TiO$_2$	CEA	0.01 pg/mL ~ 10 ng/mL	3.28 fg/mL	[22]
GQDs/PTCA−NH$_2$/Au@Fe$_3$O$_4$	miRNA-155	2.5 fM ~ 50 pM	0.83 fM	[23]
MOCs/nafion/Ru(bpy)$_3^{2+}$/GNRs	β-amyloid	10 fg/mL ~ 100 ng/mL	4.2 fg/mL	[24]

Abbreviation: GOD, glucose oxidase; CA125, carbohydrate antigen 125; PAMAM, polyamidoamine dendrimers; 5hmC, 5-hydroxymethylcytosin; VP, Vibrio parahaemolyticus; CEA, carcinoembryonic antigen; GQDs, graphene quantum dots; PTCA−NH$_2$, aminated 3,4,9,10-perylenetetracarboxylic acid; MOCs, mesoporous carbon nanospheres; bpy, 2,2-bipyridyl; GNRs, gold nanorods.
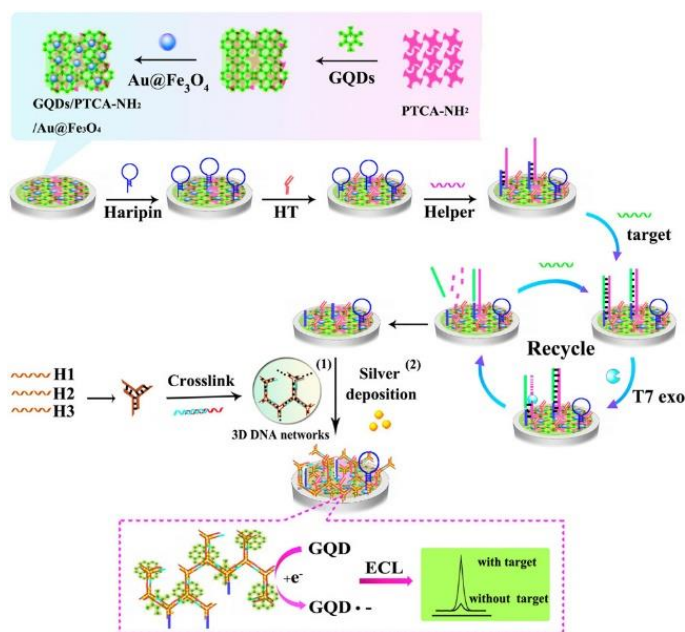

Figure 1. Schematic illustration of the solid-state GQDs-based ECL biosensor and ECL reaction mechanism for sensitive detection of miRNA [23]. Reproduced with permission. Copyright 2015, American Chemical Society.

In addition, a variety of magnetic nanomatrials have been explored as the ECL luminophores for the fabrication of novel ECL methods. Typically, Yang et al. developed a Fe$_3$O$_4$/rGO-based ECL immunosensor for the detection of carcinoembryonic antigen (CEA) by using CeO$_2$@TiO$_2$ as the ECL luminophore [22]. Zhang et al. reported an ECL method for microRNA (miRNA) detection with

graphene quantum dots (GQDs) as the ECL materials (Figure 1) [23]. In this work, GQDs were loaded on aminated 3,4,9,10-perylenetetracarboxylic acid (PTCA−NH$_2$) through π−π stacking interactions and were further modified with Fe$_3$O$_4$−Au core−shell nanocomposite (Au@Fe$_3$O$_4$) for the conjugation of DNA probes (GQDs/PTCA−NH$_2$/Au@Fe$_3$O$_4$). In the presence of target miRNA, numerous hairpin probes (HP) probes on the GQDs/PTCA−NH$_2$/Au@Fe$_3$O$_4$-modified electrode were digested with the aid of T7 exonuclease. Then, many 3D Y-shaped DNA nanostructures were tethered on the electrode surface as the templates for the in-situ generation of silver nanoparticles (AgNPs). The formed AgNPs obviously enhanced the ECL responses from GQDs.

ECL resonance energy transfer (ECL-RET) can be used as a promise strategy to develop sensitive ECL methods based on the RET interaction between a couple of acceptor and donor. For example, Ke et al. reported an immunosensor for β–amyloid detection based on ECL-RET reaction between gold nanorods (GNRs) and Ru(bpy)$_3^{2+}$ [24]. Ru(bpy)$_3^{2+}$ and antibody-modified mesoporous carbon nanospheres were immobilized on the epoxy group-functionalized Fe$_3$O$_4$ NPs. Aptamer-functionalized GNRs were used to label the captured β–amyloid. Due to the overlap of the emission spectrum of Ru(bpy)$_3^{2+}$ and adsorption spectrum of GNRs, the ECL of Ru(bpy)$_3^{2+}$ (donor) was quenched by GNRs (acceptor) through the ECL-RET process.

2.2 Carriers for capture and preconcentration of targets

In contrast to traditional methods for separation of biological species (e.g. mass-based centrifugation and size-based filtration), biological recognition elements-modified MBs can simply separate targets from complex samples to reduce the background interference with the aid of extra magnet. This method can improve the throughput of sensing system because MBs can be produced and preserved in a large-scale dose. To further improve the capture capacity toward targets, different MBs-based high-performance nanocomposites have been synthesized [25-27]. Generally, after the capture and separation, targets-modified magnetic nanocomposites were further modified with ECL probes-labeled tags. Then, the conjugates of MBs and signal tags were immobilized on the electrode surface with the help of a magnet and detected by an ECL technique [28-30].

Metal complexes can be used as the signal labels to modify the detection antibody, such as iridium (Ir) and ruthenium (Ru) complexes [31-34]. Yang et al. developed a gold nanoelectrode ensemble (Au-NEE) ECL platform by using antibody-modified MBs to capture the targets and signal reporters [35]. As shown in Figure 2, the MBs-carried sandwich conjugates with Ru(bpy)$_3^{2+}$-labeled detection antibodies as the signal reporters were attached on the Au-NEE surface by a small magnet. With carbohydrate antigen 19-9 (CA 19-9) as the model analyte, the LOD was found to be 0.4 U/mL. In contrast to the Ru(bpy)$_3^{2+}$ and luminol-H$_2$O$_2$-based ECL system at the gold macroelectrode, the sensitivity was greatly improved due to the diffusion overlap of Au-NEE and the edge effect of individual gold nanodisk. To amplify the ECL performance, nanomaterials have also be used as the anchoring matrixes to load many ECL emitters during each immunoreaction [36, 37]. For example, Zhao et al. used gold nanoparticles (AuNPs) to load tris-(2,2'-bipyridyl) ruthenium–cysteamine for the detection of protein kinase based on the magnetically-assisted ECL technology [38]. Gu et al. reported a magnetically-controlled solid-state ECL system for the detection of HeLa cells by using the branched

poly-(ethylenimine)-functionalized graphene/Fe_3O_4 hybrids to load luminol-capped AuNPs [39]. Chen et al. used MXene to carry the ECL probes (3,4,9,10-perylenetetracarboxylic acid, PTCA) for the detection of genetically modified crops [40]. Khoshfetrat et al. reported a visual ECL platform for the detection aflatoxin M1 (AFM1) by using luminol-functionalized, AgNPs-decorated GO (GO-L-AgNPs) as signal labels [41]. The AFM1 aptamer-modified AuNPs-coated Fe_3O_4 NPs (Apt-GMNPs) could bind with GO-L-AgNPs through the π-π interactions between the unpaired bases and GO. After the formation of AFM1-aptamer complexes, the GO-L-AgNPs were released from the Apt-GMNPs, resulting in the decrease of ECL signal from luminol.
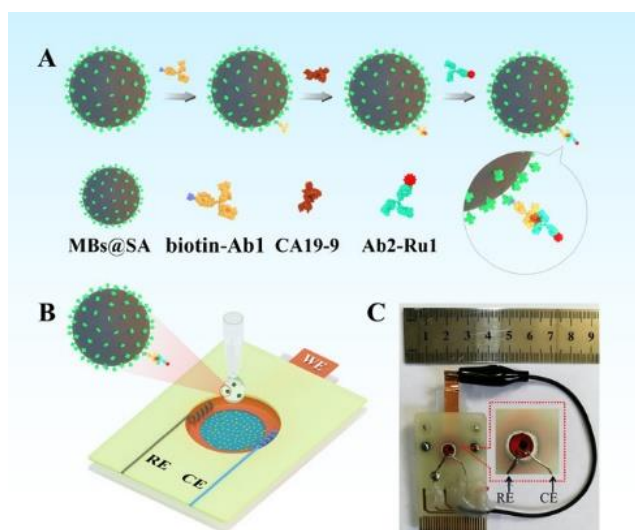

Figure 2. Schematic illustration of the principle for ECL determination of the protein biomarker CA19-9 (A) and the Au-NEE platform with immunomagnetic microbeads (B), and the photograph of the real ECL cell (C). Reproduced with permission [35]. Copyright 2020, American Chemical Society.
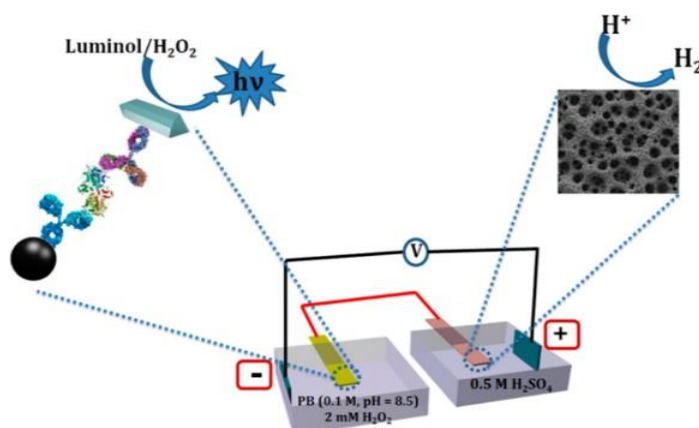
Figure 3. Schematic illustration of the amplified visual ECL detection of PSA. Reproduced with permission [42]. Copyright 2019, American Chemical Society.

A coreaction accelerator can increase the concentration of active intermediate and the ECL signal. Khoshfetrat et al. developed a visual wireless ECL immunosensor for prostate-specific antigen (PSA) detection by employing MIL-53(Fe)-NH_2 as the carrier and accelerator for luminol [42]. As

shown in Figure 3, carboxylate-modified magnetic nanoparticles (MNPs) were utilized to immobilize the primary antibody (Ab1), and the luminol-loaded MIL-53(Fe)-NH$_2$ (L@MIL-53(Fe)) were conjugated to secondary antibody (Ab2) as a signaling probe and coreaction accelerator. After the immunoreaction between Ab1, Ab2 and PSA, the sandwich immunocomplex was transferred to a gold anodic BPE and the ECL signal of luminol at the anodic poles was recorded.

The QDs-based ECL systems have been widely used in the ECL bioassays owing to its low cost, excellent optical properties and simple preparation process [43, 44]. For example, the dual-stabilizers-capped CdTe QDs have been used as the signal probes for the detection of CEA by using Fe$_3$O$_4$-Au nanocomposites as magnetic separable carriers [45]. Zhang et al. reported a universal sandwich ECL immunosensor by using magnetic Fe$_3$O$_4$@SiO$_2$ as the carrier to immobilize the capture antibody (Figure 4) [46]. In this study, the detection antibody-conjugated CdTe@ZnS QDs showing high ECL quantum yield were used as the signal tags. CEA as the model analyte was determined in the concentration range of 0.01 ~ 125 ng/mL. Moreover, to enhance the sensitivity, it is a promising strategy to embed many QDs into other nanomaterials. For instance, silica nanospheres and nanoporous PtRu alloys were used as the carriers for loading of QDs [47-50]. Carbon dots (CDs)-loaded CdTe QDs enhanced the ECL signal of QDs due to the ECL-RET process [51]. Babamiri et al. developed an ECL immunosensor for the determination of hepatitis B virus surface antigen (HBsAg) by using CdTe@CdS-PAMAM dendrimer as the ECL labels and Fe$_3$O$_4$ NPs as magnetic carriers [52]. The aminated PAMAM dendrimer was utilized as the carrier to immobilize QDs and the secondary antibody (Ab2). After the capture, separation and immobilization on the electrode, HBsAg was sensitively detected in a wide linear range from 3 fg/mL to 0.3 ng/mL. By using PAMAM dendrimer to load ruthenium complex and QDs, Babamiri et al. reported an ECL immuassay for simultaneous detection of CA125 and CA15-3 tumor markers.
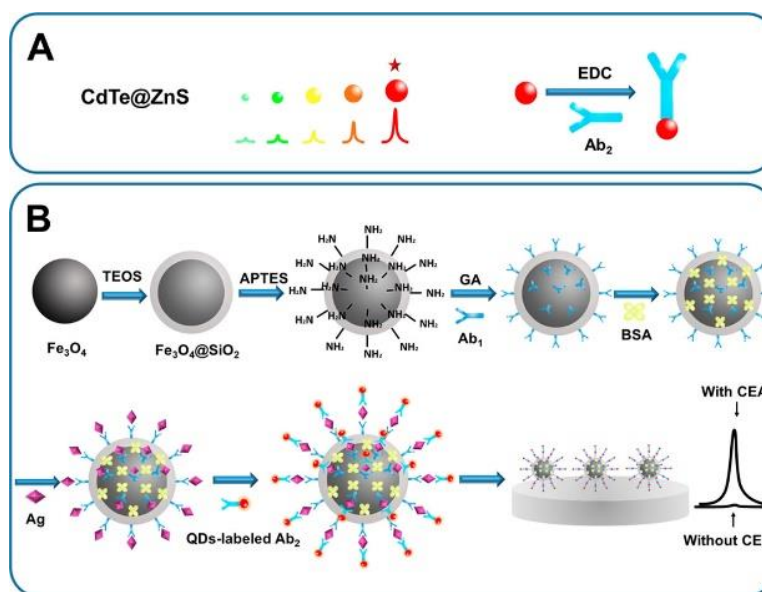

Figure 4. Schematic illustration of the preparation process of QDs-labeled Ab2 (A) and fabrication process of proposed ECL nano-immunosensor (B). Reproduced with permission [46]. Copyright 2016, American Chemical Society.

Graphene-like 2D layered nanosheet is an ideal candidate for the development of ECL sensing platforms. Because of its tunable optical-electronic properties, MoS_2 nanosheet was used as the signal quencher and ECL luminophore in ECL sensing system. For example, Shi et al. reported a magnetic ECL sensing platform with luminous MoS_2 nanosheet as the ECL emitter [53]. In this work, the hairpin aptamer-labeled magnetic vesicle was utilized to capture the target miRNA. After magnetic separation, the captured target triggered the catalyzed hairpin assembly, which allowing for the capture of probe DNA-modified MoS_2 by hybridization. The target concentration was then determined by monitoring the ECL signal change on a magnetic electrode. Graphite-like carbon nitride (g-C_3N_4) nanosheet is an effective ECL emitter. Recently, Khoshfetrat et al. designed a closed split bipolar ECL sensing platform for the simultaneous detection of gene-specific methylation by using luminol-loaded Fe_3O_4@UiO-66 and gold nanorod-functionalized graphite-like carbon nitride nanosheet (AuNRs@C_3N_4 NS) as the ECL signal labels [54]. As shown in Figure 5, in the presence of the *SLC5A8* gene, the anti-5mC monoclonal antibody (anti-5mC)-modified AuNRs@C_3N_4 NSs were immobilized on the electrode. The complementary capture DNA probe modified on L-Fe_3O_4@UiO-66 was hybridized with *RASSF1A* gene, facilitating the capture of signal labels onto the anti-5mC-anodic-modified electrode.
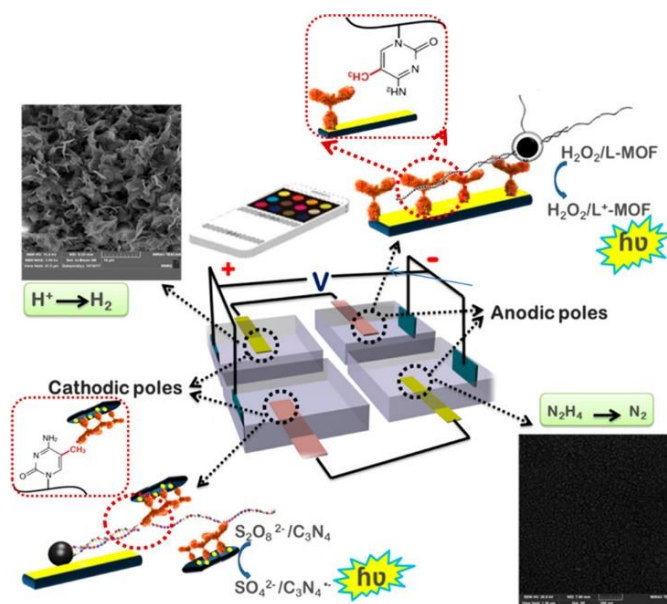
Figure 5. Schematic illustration of amplified simultaneous visual-based detection of *RASSF1A* and *SLC5A8* tumor suppressor gene methylation. Reproduced with permission [54]. Copyright 2022, American Chemical Society.

DNA-based molecular machines have been considered as powerful signal amplification strategies for bioanalysis, including DNA hybridization-based assembly and enzymes-based amplification. MBs can act as the amplification station for the DNA-based molecular machines [55]. Chen et al. reported an ECL aptasensor for tumor cell detection based on rolling circle amplification (RCA) occurred on the surface of aptamer-modified Au-Fe_3O_4 NPs [56]. The RCA products could adsorb a large number of ruthenium complex and then be trapped by magnetic electrode for the ECL detection. Recently, different DNA-based nanostructures have been designed as signal amplifiers for biosensing analysis. For example, Zhang et al. reported an ECL immunosensor for the detection of

histone acetyltransferase (HAT p300) by using magnetic AuNPs Au-Fe$_3$O$_4$ NPs as the electrode modifiers and pure DNA nano-frameworks as the signal amplifiers [57]. In this work, the acetyl antibody (AbAc)-conjugated DNA nanonets and terminal deoxynucleotidyl transferase (TdT)-triggered renascent DNAs (AT-dsDNAs) were used as the signal tags. A large number of Ru(phen)$_3^{2+}$ molecules as the luminophores were integrated into the DNA nanomaterials, thus producing a strong ECL signal.

Table 2. Detection performances of ECL biosensors by using MBs for the capture and preconcentration of targets.

Signal label	Target	Linear range	LOD	Ref.
Ru(bpy)$_3^{2+}$-labeled DNA	ORF1ab Gene	0.1 fM ~ 10 µM	0.1 fM	[29]
Ru(bpy)$_3^{2+}$-doped silica/AuNPs	hemoglobin	0.1 pg/mL ~ 40 ng/mL	23 fg/mL	[32]
Ru complex-labeled antibody	D-Dimer antigen	2.5 ~ 40 ng/mL	1 ng/mL	[33]
Ru(bpy)$_2$(phen-5-NH$_2$) (PF6)$_2$	5hmC	0.01 ~ 500 nM	2.86 pM	[34]
Ru(bpy)$_3^{2+}$-doped silica	H9N2 virus	25 fg/mL ~ 25 ng/mL	14 fg/mL	[36]
Ru(bpy)$_3^{2+}$-doped silica	CEA	10 fg/mL ~ 10 ng/mL	3.5 fg/mL	[37]
Ru complex-labeled AuNPs	protein kinase	0.01 ~ 50 U/mL	5 mU/mL	[38]
Luminol-AuNPs	HeLa cells	20 ~ 1 × 10^4 cells/mL	8 cells	[39]
MXene-PTCA	Cry1Ab	0.005 ~ 100 ng/mL	1 pg/mL	[40]
GO-luminol-AgNPs	aflatoxin M1	5 ~ 150 ng/mL	0.05 ng/mL	[41]
Luminol-MIL-53(Fe)-NH$_2$	PSA	0.001 ~ 300 ng/mL	0.2 pg/mL	[42]
Ru complex-labeled antibody	CA 19-9	0.5 ~ 20 U/mL	0.4 U/mL	[35]
CdTe QDs-labeled antibody	HSA	10 ~ 480 ng/mL	10 ng/mL	[43]
CdTe QDs-labeled antibody	CEA	0.005 ~ 80 ng/mL	1 pg/mL	[45]
CdTe@ZnS QDs-labeled antibody	CEA	0.01 ~ 125 ng/mL	3 pg/mL	[46]
CdTe QDs coated SiO$_2$	PSA	0.003 ~ 50 ng/mL	0.72 pg/mL	[47]
mSiO$_2$/CdTe QDs	CEA	0.001 ~ 80 ng/mL	0.3 pg/mL	[49]
mSiO$_2$/CdTe QDs	miRNAs	0.1 ~ 100 pM	33 fM	[50]
CdTe@CDs	SCCA	0.02 ~ 12 ng/mL	6.3 fg/mL	[51]
CdTe@CdS-PAMAM dendrimer	HBsAg	3 fg/mL ~ 0.3 ng/mL	0.08 fg/mL	[52]
MoS$_2$ nanosheet	miRNA-210	1 fM ~ 100 pM	0.3 fM	[53]
Ru complex-labeled DNA	Ramos cells	20 ~ 500 cells	16 cells	[56]
Ru complex	HAT	0.006 ~ 60 nM	2.9 pM	[57]

Abbreviation: AuNPs, gold nanoparticles; 5hmC, 5-hydroxymethylcytosine; CEA, carcinoembryonic antigen; PTCA, 3,4,9,10-perylenetetracarboxylic acid; GO, graphene oxide; PSA, prostate-specific antigen; CA 19-9, carbohydrate antigen 19-9; HSA, human serum albumin; CDs, carbon dots; SCCA, squamous cell carcinoma antigen; HBsAg, hepatitis B virus surface antigen; HAT, histone acetyltransferase.

2.3 MBs-based homogeneous ECL biosensors

In the MBs-based homogeneous methods, the targets can interact with the recognition elements modified on the MBs in a homogeneous medium and then release certain mediate species (e.g. enzymes products and messenger DNA) that can be further determined by various ECL methods. For instance, Jin et al. reported a magnetic graphene oxide (GO)-based ECL aptasensor for thrombin, in which thrombin could induce the release of iridium complex-modified aptamer from the GO surface [58]. Up

to date, many DNA amplifiers with well biomolecule transduction and excellent amplification ability have been integrated into ECL bioassays, such as strand-displacement amplification (SDA) and hybrid chain reaction (HCR) [59, 60]. Thus, it is an effective way to convert a target into a messenger DNA probe for the next ECL detection [61, 62]. For example, Dai et al. reported an ECL biosensor for cell detection by combing the MBs-based target conversion with isothermal circular double-assisted signal amplification [63]. Jie et al. developed an ECL biosensor for the detection of cancer cells with magnetic quantum dot (QD) composites as the signal labels [64]. The target cells induced the release of DNA (s1) from the aptamer-modified MBs. The capture DNA probes were immobilized on the GO-modified electrode for the anchoring of magnetic QD composites. Through the endonuclease-assisted amplification process, many captured QD composites were released from the electrode, significantly causing the ECL signal change induced by target cells.

HCR is an attractive signal amplification strategy without enzyme participation [65]. Hao et al. reported an ECL biosensor for the detection of miRNAs by combing anti-fouling MBs with DNAzyme-assisted target recycling amplification and HCR [66]. As shown in Figure 6, in the presence of miRNA-21, three-chain structures formed on the surface of MBs. Mn^{2+} ions triggered the DNAzyme-assisted target recycling amplification and many short single DNA strands were released as the output DNA probes to initiate the HCR process on the electrode surface. The positively charged ruthenium complexes were inserted into the DNA polymers to generate a strong ECL signal. To avoid the complex and time-consuming immobilization process, homogeneous ECL detection strategies are highly desired due to their high efficiency and reproducibility. Li et al. developed a homogeneous ECL biosensor for flap endonuclease 1 (FEN1) detection with double-flap DNA-modified MBs as the reaction platforms [67]. The double-flap DNA contained a 5′-flap. In the presence of FEN1, the 5′-flap was cut, thus producing many ssDNA chains. The cut 5′-flap was further used to initiate branched hybridization chain reaction (BHCR) amplification, leading to the formation of double DNA stands (dsDNAs) with a large 3D structure and high molecular weight. The $Ru(phen)_3^{2+}$ molecules were embedded in the dsDNAs and then separated by ultrafiltration. The ECL signal from the $Ru(phen)_3^{2+}$-dsDNAs increased linearly with the increase of the logarithm of FEN1 concentration.
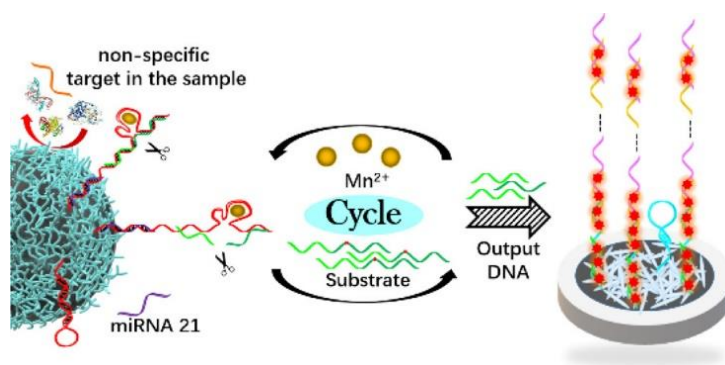

Figure 6. Schematic illustration of the sensing process of the detection of miRNA-21. Reproduced with permission [66]. Copyright 2021, American Chemical Society.

DNA nanomachines have also be used as the signal labels to design MBs-based homogeneous ECL biosensors. For example, Hu et al. reported an ECL biosensor with DNA-labeled MBs (DNA-MBs)

Int. J. Electrochem. Sci., 17 **(2022)** Article Number: 221189

10

to produce a large number of output DNA probes [68]. The self-enhanced NCNDs-BPEI-Ru nanocomposites as the ECL signal probes were modified on the PtNPs/Nafion electrode. The methylene blue-embedded self-assembled DNA nanotubes were recruited by the capture DNA probe-modified electrode through hybridization reaction.
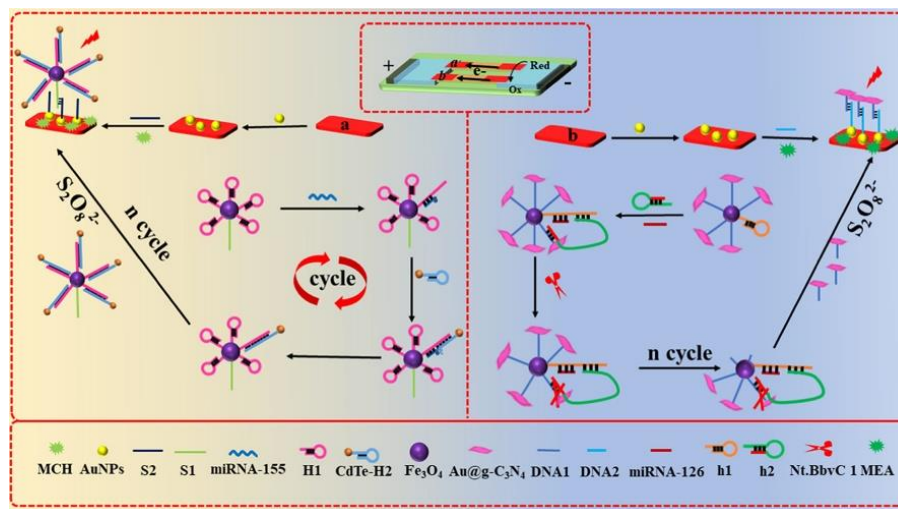

Figure 7. Schematic illustration of preparation of the paper-based potential-resolved BPE-ECL biosensor for the detection of miRNA-155 and miRNA-126. Reproduced with permission [69]. Copyright 2021, American Chemical Society.

Table 3. Detection performances of MBs-based homogeneous ECL biosensors.

Signal label	Target	Linear ranges	LOD	Ref.
Ir complex-labeled DNA	thrombin	2 ~ 50 nM	1.3 nM	[58]
Ru complex-labeled DNA	okadaic acid	0.01 ~ 10 ng/mL	4 pg/ml	[59]
AgNP-Pyc@MMSNs	Amacr	0.01 ~ 100 μg/mL	1.25 ng/mL	[60]
QD nanocluster	cancer cells	160 ~ 15360 cells/mL	89 cells/mL	[61]
ABEI-labeled DNA	microRNA-21	1 aM ~ 100 pM	0.33 aM	[62]
CdS QDs	HL-60 cancer cells	10 ~ 5000 cells	10 cells	[63]
QDs-labeled DNA	Cancer cells	300 ~ 9000 cells/mL	98 cells/mL	[64]
Pe@Ag MFs	K-ras gene	50 fM ~ 10 nM	5.1 fM	[65]
$Ru(bpy)_2(cpaphen)^{2+}$	microRNA-21	1 fM ~ 1 nM	0.13 fM	[66]
$Ru(phen)_3^{2+}$	flap endonuclease 1	0.065 ~ 6500 U/L	22 mU/L	[67]
NCNDs-BPEI-Ru	DNA	50 aM ~1 nM	1.4 aM	[68]
CdTe QDs and Au@g-C_3N_4 NSs	miRNA-155 and miRNA-126	10 fM ~ 0.1 μM	5.7 and 4.2 fM	[69]

Abbreviation: AgNPs, silver nanoparticles; Pyc, 1-pyrenecarboxaldehyde; MMSNs, magnetic mesoporous silica nanoparticles; Amacr, alpha-methylacyl-CoA racemase; ABEI, N-(4-aminobutyl)-N-ethylisoluminol; Pe@Ag MFs, perylene decorated Ag microflowers; bpy, 2,2'-bipyridy; cpaphen, 5-amino-1,10-phenanthroline; NCNDs, nitrogen-doped carbon nanodots; BPEI, branched polyethyleneimine.

In the presence of output DNA probes, the self-assembled DNA nanotubes would be disintegrated, thus leading to the release of methylene blue and the recovery of ECL signal. The signal-

on biosensor could determine mycobacterium tuberculosis with a LOD down to 1.4 aM. Moreover, 3D DNA nanomachines have been aroused wide interest by running on 3D nanomaterials. Wang et al. designed a potential-resolved paper-based ECL platform for simultaneous detection of multiple miRNAs by using magnetic Fe_3O_4 as the carrier of two nanoprobes (CdTe QDs-H2 and Au@g-C_3N_4-DNA1) (Figure 7) [69]. The CdTe QDs-H_2/$S_2O_8^{2-}$ and Au@g-C_3N_4-DNA1/$S_2O_8^{2-}$ systems showed two ECL emissions at a drive voltage of 9 and 12 V, respectively. In this method, the integration of bipolar electrode system and potential-resolved multi-target strategy significantly reduced the spatial interference. Moreover, the ECL signal was amplified by the 3D DNA nanomachine and the target-triggered cycling.

2.4 Signal labels

MBs with a large surface area can be used as the carriers to load luminescent materials for signal amplification [70]. For example, Yang et al. employed palladium nanoparticle-functionalized graphene-aerogel-supported Fe_3O_4 as a novel carrier to load large amounts of $Ru(bpy)_3^{2+}$ via electrostatic interaction for the immunosensing of PSA [71]. Tang et al. proposed an ECL strategy for monitoring the level of epidermal growth factor receptor (EGFR) on MCF-7 cells by using epidermal growth factor (EGF)-modified CdS QDs-capped MBs as the signal probes [72]. Zhou et al. proposed an ECL strategy for the detection of multiple latent tuberculosis infection (LTBI) biomarkers by using carbon quantum dots (CQDs) and luminol–capped AuNPs–modified MBs (MB@Au@CQDs and MB@Au@luminol) as the signal probes [73].
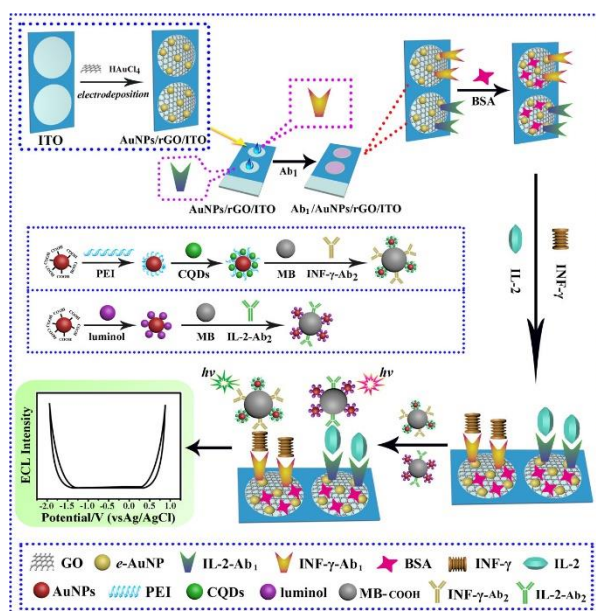

Figure 8. Schematic illustration of preparation process of the ECL-sensing platform for the determination of IFN-γ and IL-2. Reproduced with permission [73]. Copyright 2017, American Chemical Society.

Figure 9. Schematic illustration of proposed ECL immunosensor for NT-proBNP determination. Reproduced with permission [74]. Copyright 2017, American Chemical Society.

Table 4. Detection performances of different ECL biosensors by using MBs as the signal labels.

Signal label	Target	Linear range	LOD	Ref.
bi-Arg/Au@Fe_3O_4–rGO	APE1	1 fg/mL ~ 50 pg/mL	0.3 fg/mL	[70]
Ru@FGA-Pd	PSA	0.1 pg/mL ~ 50 ng/mL	0.056 pg/mL	[71]
CdS ODs-capped MBs	EGFR	80 ~ 4 ×10^6 cells/mL	40 cells/mL	[72]
MB@Au@CQDs and MB@Au@luminol	IFN-γ and IL-2	10 fg/mL ~ 1000 pg/mL	10 pg/mL	[73]
Fe_3O_4@PDA	NT-proBNP	0.5 pg/mL ~ 100 ng/mL	0.28 pg/mL	[74]
Patchy Au coated Fe_3O_4	CEA	0.1 pg/mL ~15 ng/mL	0.03 pg/mL	[75]
Luminol–AuNPs@Fe_3O_4	mucin-1	10 fg/mL ~ 10 ng/mL	4.5 fg/mL	[76]
Fe_3O_4−CeO_2	Cyclin-D1	50 fg/mL ~ 50 ng/mL	28 fg/mL	[77]

Abbreviation: bi-Arg, bi-arginine; rGO, reduced graphene oxide; APE1, Apurinic/apyrimidinic endonuclease 1; Ru@FGA-Pd, $Ru(bpy)_3^{2+}$ and palladium nanoparticle-functionalized graphene-aerogel-supported Fe_3O_4; PSA, prostate specific antigen; EGFR, epidermal growth factor receptor; MBs, magnetic beads; CQDs, carbon quantum dots; IFN-γ, interferon-gamma; IL-2, interleukin-2; PDA, polydopamine; NT-proBNP, N-terminal proB-type natriuretic peptide; CEA, carcinoembryonic antigen.

As shown in Figure 8, AuNPs were electrodeposited on the GO-modified ITO electrode for the immobilization of the capture antibodies of two LTBI biomarkers (IFN-γ and IL-2). The captured targets were recognized by the detection antibody-labeled MB@Au@CQDs and MB@Au@luminol. Polydopamine (PDA) was always used as the shell to prepare core-shell nanocomposite, which can improve the stability and facilitate the conjugation with biomolecules. Shi et al. reported a sandwich ECL immunosensor for the detection of N-terminal proB-type natriuretic peptide (NT-proBNP) with PDA–coated Fe_3O_4 as the quencher and the carrier of detection antibody [74]. As presented in Figure 9, the AuNP-modified GO-$Ru(bpy)_3^{2+}$/$Ag_2C_2O_4$ nanocomposite was employed as the luminophore and the platform for the immobilization of capture antibody. After the formation of sandwich immunocomplex, the excited state of $Ru(bpy)_3^{2+}$ was quenched by the quinone unit in PDA through energy transfer.

MBs with the peroxidase-like ability can act as the coreation accelerators to promote the reduction of coreactant. Moreover, the nanocomposite of MBs and other nanomaterials have been prepared to further enhance the catalytic effect [75]. For instance, Wang et al. developed an ECL immunosensor by using luminol–covered AuNP–modified Fe_3O_4 (luminol-AuNP@Fe_3O_4) to label the detection antibody [76]. The luminol-AuNPs were prepared by the reduction of $HAuCl_4$ with $NaBH_4$ as the reducing reagent in the presence of luminol. The luminol-AuNPs were adsorbed onto the Fe_3O_4 surface by electrostatic interactions to produce Lu–AuNPs@Fe_3O_4 nanocomposites. In this work, Fe_3O_4 showed high catalytic activity for H_2O_2 decomposition, thus enhancing the sensitivity of luminol–H_2O_2 system. Zhou et al. demonstrated that the Fe_3O_4-CeO_2 nanocomposite as the coreaction accelerator can improve the ECL signal of the silver nanocluster (AgNCs)/$S_2O_8^{2-}$ system (Figure 10) [77]. In this work, the in-situ electrogenerated AgNC acted as the ECL emitter. The ECL luminous efficiency was greatly improved by using Fe_3O_4-CeO_2 to accelerate the reduction of $S_2O_8^{2-}$ and the generation of the intermediate radical $SO_4^{\cdot-}$. The method could detect Cyclin-D1 (CCND1) with a linear range of 50 fg/mL ~ 50 ng/mL and a LOD of 28 fg/mL. CCND1 is overexpressed on the surface of MCF-7 cancer cells. The ECL biosensor was further used to evaluate the efficiency of sophorae to MCF-7 cells.
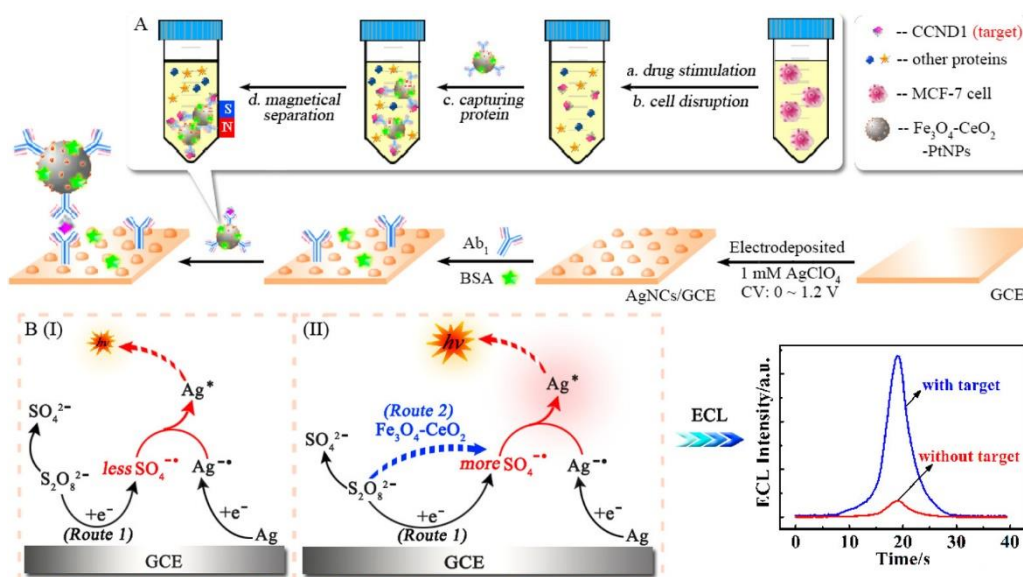

Figure 10. Schematic illustration of proposed AgNCs-based ECL immunosensor for cancer cells determination. Reproduced with permission [77]. Copyright 2017, American Chemical Society.

3. CONCLUSION

In this review, we summarized the progress in the design and application of magnetically-assisted ECL biosensors. Generally, the magnetic materials have been used as the electrode materials to increase the sensing interface surface, and/or as the carries to capture and separate the targets or load the signal reporters. The analytical performances including detection limit, linear range and the roles of magnetic

materials in the sensing systems were compared in the tables. This work would be helpful for the design of novel ECL sensing platforms to detect various biomarkers.

References

1. X. Ma, W. Gao, F. Du, F. Yuan, J. Yu, Y. Guan, N. Sojic and G. Xu, *Acc. Chem. Res.*, 54 (2021) 2936.
2. X. Chen, B. Su, X. Song, Q. Chen, X. Chen and X. Wang, *TrAC-Trend. Anal. Chem.*, 30 (2011) 665.
3. E. Yang, Y. Zhang and Y. Shen, *Anal. Chim. Acta*, 1209 (2022) 339140.
4. H. Qi, Y. Peng, Q. Gao and C. Zhang, *Sensors*, 9 (2009) 674.
5. E. Martinez-Perinan, C. Gutierrez-Sanchez, T. Garcia-Mendiola and E. Lorenzo, *Biosensors*, 10 (2020) 118.
6. K. M. Koo, N. Soda and M. J. A. Shiddiky, *Curr. Opin. Electrochem.*, 25 (2021) 100645-100652.
7. Y. Xu and E. Wang, *Electrochim. Acta*, 84 (2012) 62.
8. M. Pastucha, Z. Farka, K. Lacina, Z. Mikusova and P. Skladal, *Microchim. Acta*, 186 (2019) 312.
9. T. Kavetskyy, M. Alipour, O. Smutok, O. Mushynska, A. Kiv, D. Fink, F. Farshchi, E. Ahmadian and M. Hasanzadeh, *Microchem. J.*, 167 (2021) 106320.
10. J. Qian, K. Wang, Y. Jin, X. Yang, L. Jiang, Y. Yan, X. Dong, H. Li and B. Qiu, *Biosens. Bioelectron.*, 57 (2014) 149.
11. Y. Shen, X. Qian, X. Mi and Y. Tu, *Bioelectrochemistry*, 145 (2022) 108086.
12. Q. Xu, J. Li, S. Li and H. Pan, *J. Solid State Electrochem.*, 16 (2012) 2891.
13. R.-R. Zhang, J. Zhan, J.-J. Xu, J.-Y. Chai, Z.-M. Zhang, A.-L. Sun, J. Chen and X.-Z. Shi, *Sens. Actuat. B: Chem.*, 317 (2020) 128237.
14. P. Tong, Y. Meng, J. Liang and J. Li, *Sens. Actuat. B: Chem.*, 330 (2021) 129405-129412.
15. J. Zhou, N. Gan, T. Li, F. Hu, X. Li, L. Wang and L. Zheng, *Biosens. Bioelectron.*, 54 (2014) 199.
16. J. Li, Q. Xu, C. Fu and Y. Zhang, *Sens. Actuat. B: Chem.*, 185 (2013) 146.
17. H. Shao, J. Lu, Q. Zhang, Y. Hu, S. Wang and Z. Guo, *Sens. Actuat. B: Chem.*, 268 (2018) 39.
18. W. Jiang, L. Wu, J. Duan, H. Yin and S. Ai, *Biosens. Bioelectron.*, 99 (2018) 660.
19. T. Wang, X. Song, H. Lin, T. Hao, Y. Hu, S. Wang, X. Su and Z. Guo, *Anal. Chim. Acta*, 1062 (2019) 124.
20. Y. M. Lei, B. Q. Xiao, W. B. Liang, Y. Q. Chai, R. Yuan and Y. Zhuo, *Biosens. Bioelectron.*, 109 (2018) 109.
21. H. Hai, C. Chen, D. Chen, P. Li, Y. Shan and J. Li, *Microchim. Acta*, 188 (2021) 125.
22. L. Yang, W. Zhu, X. Ren, M. S. Khan, Y. Zhang, B. Du and Q. Wei, *Biosens. Bioelectron.*, 91 (2017) 842.
23. P. Zhang, Y. Zhuo, Y. Chang, R. Yuan and Y. Chai, *Anal. Chem.*, 87 (2015) 10385.
24. H. Ke, H. Sha, Y. Wang, W. Guo, X. Zhang, Z. Wang, C. Huang and N. Jia, *Biosens. Bioelectron.*, 100 (2018) 266.
25. Y. Hu, L. Su, S. Wang, Z. Guo, Y. Hu and H. Xie, *Microchim. Acta*, 186 (2019) 512.
26. L. Su, J. Mao, S. Wang and Y. Hu, *J. Electroanal. Chem.*, 873 (2020) 114376.
27. Y. Xiao, S. Chen, S. Zhang, G. Wang, H. Yi, G. Z. Xin and X. Yang, *Talanta*, 231 (2021) 122399.
28. W. Shao, *Int. J. Electrochem. Sci.*, 12 (2017) 11506.
29. C. Jiang, X. Mu, S. Liu, Z. Liu, B. Du, J. Wang and J. Xu, *Sensors*, 22 (2022) 2402.
30. G. Valenti, E. Rampazzo, E. Biavardi, E. Villani, G. Fracasso, M. Marcaccio, F. Bertani, D.

Ramarli, E. Dalcanale, F. Paolucci and L. Prodi, *Faraday. Discuss.*, 185 (2015) 299.
31. M. Zhou and Y. Xia, *Anal. Chim. Acta*, 1023 (2018) 29.
32. J. Zhou, N. Gan, F. Hu, T. Li, H. Zhou, X. Li and L. Zheng, *Sens. Actuat. B: Chem.*, 186 (2013) 300.
33. Y. Wei, Y. Wang, J. Wang, X. Yang, H. Qi, Q. Gao and C. Zhang, *Anal. Bioanal. Chem.*, 411 (2019) 4203.
34. C. Sui, H. Yin, L. Wang, Y. Zhou and S. Ai, *Biosens. Bioelectron.*, 150 (2020) 111908.
35. X. Yang, Y. Wei, Y. Du, H. Qi, Q. Gao and C. Zhang, *Anal. Chem.*, 92 (2020) 15837.
36. F. Luo, C. Long, Z. Wu, H. Xiong, M. Chen, X. Zhang, W. Wen and S. Wang, *Sens. Actuat. B: Chem.*, 310 (2020) 127831.
37. G. Jie, J. Ge, X. Gao and C. Li, *Biosens. Bioelectron.*, 118 (2018) 115.
38. Z. Zhao, X. Zhou and D. Xing, *Biosens. Bioelectron.*, 31 (2012) 299.
39. W. Gu, X. Deng, X. Gu, X. Jia, B. Lou, X. Zhang, J. Li and E. Wang, *Anal. Chem.*, 87 (2015) 1876.
40. X. Chen, D. Zhang, H. Lin, W. Wei, T. Hao, Y. Hu, S. Wang and Z. Guo, *Sens. Actuat. B: Chem.*, 346 (2021) 130549.
41. S. M. Khoshfetrat, H. Bagheri and M. A. Mehrgardi, *Biosens. Bioelectron.*, 100 (2018) 382.
42. S. M. Khoshfetrat, H. Khoshsafar, A. Afkhami, M. A. Mehrgardi and H. Bagheri, *Anal. Chem.*, 91 (2019) 6383.
43. B. Y. Liao, C. C. Cheng, C. F. Wang, C. H. Lu and J. K. Chen, *Biosens. Bioelectron.*, 183 (2021) 113240.
44. B.-Y. Liao, C.-J. Chang, C.-F. Wang, C.-H. Lu and J.-K. Chen, *Sens. Actuat. B: Chem.*, 336 (2021) 129710.
45. X. Zhang and S.-N. Ding, *Sens. Actuat. B: Chem.*, 240 (2017) 1123.
46. X. Zhang and S.-N. Ding, *ACS Sens.*, 1 (2016) 358.
47. F. Liu, Y. Zhang, S. Ge, J. Lu, J. Yu, X. Song and S. Liu, *Talanta*, 99 (2012) 512.
48. Y. Zhang, S. Ge, S. Wang, M. Yan, J. Yu, X. Song and W. Liu, *Analyst*, 137 (2012) 2176.
49. H. Dong, T.-T. Han, L.-L. Ren and S.-N. Ding, *J. Electroanal. Chem.*, 806 (2017) 32.
50. H. Y. Zhu and S. N. Ding, *Biosens. Bioelectron.*, 134 (2019) 109.
51. S. Li, J. Luo, X. Yang, Y. Wan and C. Liu, *Sens. Actuat. B: Chem.*, 197 (2014) 43.
52. B. Babamiri, R. Hallaj and A. Salimi, *Sens. Actuat. B: Chem.*, 254 (2018) 551.
53. J. Shi, Y. Zhang, P. Wang, Y. Nie and Q. Ma, *Talanta*, 237 (2022) 122969.
54. S. M. Khoshfetrat, P. Seyed Dorraji, M. Shayan, F. Khatami and K. Omidfar, *Anal. Chem.*, 94 (2022) 8005.
55. M. H. Shamsi, K. Choi, A. H. Ng, M. D. Chamberlain and A. R. Wheeler, *Biosens. Bioelectron.*, 77 (2016) 845.
56. M. Chen, S. Bi, X. Jia and P. He, *Anal. Chim. Acta*, 837 (2014) 44.
57. Q. Zhang, D. Hu, T. Zhan, Y. Hu, Z. Guo and S. Wang, *Sens. Actuat. B: Chem.*, 316 (2020) 128165.
58. G. Jin, L. Lu, X. Gao, M.-J. Li, B. Qiu, Z. Lin, H. Yang and G. Chen, *Electrochim. Acta*, 89 (2013) 13.
59. W. Yang, G. Zhang, J. Ni, Q. Wang and Z. Lin, *Sens. Actuat. B: Chem.*, 327 (2021) 128872.
60. M.-L. Liu, Y. Li, M.-L. Zhao, Y. Zhuo and X.-J. He, *Biosens. Bioelectron.*, 214 (2022) 114512.
61. G. Jie, J. Zhang, G. Jie and L. Wang, *Biosens. Bioelectron.*, 52 (2014) 69.
62. Y. Zhang, Y. Chai, H. Wang and R. Yuan, *Anal. Chem.*, 91 (2019) 14368.
63. P. P. Dai, J. Y. Li, T. Yu, J. J. Xu and H. Y. Chen, *Talanta*, 141 (2015) 97.
64. G. Jie, Y. Zhao and S. Niu, *Biosens. Bioelectron.*, 50 (2013) 368.
65. F. Yang, Y. W. He, Y. Q. Chai, R. Yuan and Y. Zhuo, *Biosens. Bioelectron.*, 182 (2021) 113178.
66. Q. Hao, Q. Xu, S. Niu, C. Ding and X. Luo, *Anal. Chem.*, 93 (2021) 10679.
67. X. Li, Y. Huang, J. Chen, S. Zhuo, Z. Lin and J. Chen, *Bioelectrochemistry*, 147 (2022) 108189.
68. J. Hu, Y. Zhang, Y. Chai and R. Yuan, *Sens. Actuat. B: Chem.*, 354 (2022) 131252.
69. F. Wang, Y. Liu, C. Fu, N. Li, M. Du, L. Zhang, S. Ge and J. Yu, *Anal. Chem.*, 93 (2021) 1702.

70. M. Zhao, X. D. Chai, J. Han, G. F. Gui, R. Yuan and Y. Zhuo, *Anal. Chim. Acta*, 846 (2014) 36.
71. L. Yang, Y. Li, Y. Zhang, D. Fan, X. Pang, Q. Wei and B. Du, *ACS Appl. Mater. Interfaces*, 9 (2017) 35260.
72. Y. Tang, S. Zhang, Q. Wen, H. Huang and P. Yang, *Anal. Chim. Acta*, 881 (2015) 148.
73. B. Zhou, M. Zhu, Y. Qiu and P. Yang, *ACS Appl. Mater. Interfaces*, 9 (2017) 18493.
74. L. Shi, X. Li, W. Zhu, Y. Wang, B. Du, W. Cao, Q. Wei and X. Pang, *ACS Sens.*, 2 (2017) 1774.
75. X. Zhang, N. Bao, X. Luo and S. N. Ding, *Biosens. Bioelectron.*, 114 (2018) 44.
76. J. X. Wang, Y. Zhuo, Y. Zhou, R. Yuan and Y. Q. Chai, *Biosens. Bioelectron.*, 71 (2015) 407.
77. Y. Zhou, M. Chen, Y. Zhuo, Y. Chai, W. Xu and R. Yuan, *Anal. Chem.*, 89 (2017) 6787